PNAS RESEARCH ARTICLE | MEDICAL SCIENCES

Claudin-2 upregulation enhances intestinal permeability, immune activation, dysbiosis, and mortality in sepsis

Takehiko Oami[a,b,1], Shabnam Abtahi[c,1], Takashi Shimazui[a,b], Ching-Wen Chen[a], Yan Y. Sweat[c], Zhe Liang[a], Eileen M. Burd[d], Alton B. Farris[d], Joe T. Roland[e], Sachiko Tsukita[f], Mandy L. Ford[g], Jerrold R. Turner[c,2], and Craig M. Coopersmith[a,2]

Edited by Timothy R. Billiar, University of Pittsburgh Medical Center, Pittsburgh, PA; received October 19, 2022; accepted January 16, 2024 by Editorial Board Member Carl F. Nathan

Intestinal epithelial expression of the tight junction protein claudin-2, which forms paracellular cation and water channels, is precisely regulated during development and in disease. Here, we show that small intestinal epithelial claudin-2 expression is selectively upregulated in septic patients. Similar changes occurred in septic mice, where claudin-2 upregulation coincided with increased flux across the paracellular pore pathway. In order to define the significance of these changes, sepsis was induced in claudin-2 knockout (KO) and wild-type (WT) mice. Sepsis-induced increases in pore pathway permeability were prevented by claudin-2 KO. Moreover, claudin-2 deletion reduced interleukin-17 production and T cell activation and limited intestinal damage. These effects were associated with reduced numbers of neutrophils, macrophages, dendritic cells, and bacteria within the peritoneal fluid of septic claudin-2 KO mice. Most strikingly, claudin-2 deletion dramatically enhanced survival in sepsis. Finally, the microbial changes induced by sepsis were less pathogenic in claudin-2 KO mice as survival of healthy WT mice injected with cecal slurry collected from WT mice 24 h after sepsis was far worse than that of healthy WT mice injected with cecal slurry collected from claudin-2 KO mice 24 h after sepsis. Claudin-2 upregulation and increased pore pathway permeability are, therefore, key intermediates that contribute to development of dysbiosis, intestinal damage, inflammation, ineffective pathogen control, and increased mortality in sepsis. The striking impact of claudin-2 deletion on progression of the lethal cascade activated during sepsis suggests that claudin-2 may be an attractive therapeutic target in septic patients.

sepsis | gut | intestine | barrier | tight junction

Significance

Sepsis is responsible for nearly 20% of deaths worldwide. Current therapy for sepsis is restricted to antibiotics directed toward the initiating pathogen, combined with non-specific supportive care. There are no approved therapies aimed at the dysregulated host response which plays a critical role in the development of multiple organ dysfunction and mortality from sepsis. In this study, we found that small intestinal epithelial claudin-2 expression is selectively upregulated in septic patients. Mortality due to sepsis is markedly reduced in claudin-2 knockoot mice, which is, at least partly, due to claudin-2-dependent effects on sepsis-induced dysbiosis. Claudin-2 and its effects on the microbiome may be attractive therapeutic targets in sepsis.

Sepsis is responsible for nearly 20% of deaths worldwide (1). In the United States, forty percent of Medicare patients with septic shock die while in the hospital or within a week of discharge, and the costs of sepsis for Medicare beneficiaries may exceed $62 billion, more than double previous estimates (2). Despite these sobering realities, current therapy for sepsis is restricted to antibiotics, fluid resuscitation, and supportive care (3). Although protocols emphasizing early management have been associated with decreased mortality (4), a meta-analysis of over 200 randomized trials demonstrated only a small improvement in patient outcomes in sepsis (5).

The gut has long been hypothesized to play a critical role in the pathogenesis of sepsis and has been referred to as the "motor" of the systemic inflammatory response in sepsis (6–8). The intestinal epithelium is a single cell layer that separates the host from the diverse microbial populations within the gut lumen (9). Under basal conditions, the epithelial barrier allows paracellular movement of water, solutes, and immune-modulating factors while largely restricting pathogens to the gut lumen (10). This barrier function, which is compromised in critically ill patients and pre-clinical sepsis models, has been proposed to allow luminal materials to alter the host inflammatory response and propagate systemic disease (11–13). This may take on increased significance given the dysbiosis that is associated with increased mortality in septic patients and is also associated with mortality in pre-clinical sepsis models (14–18).

Paracellular permeability, the converse of barrier function, is defined by the apical tight junction (13). Two distinct modes of tight junction permeability can be regulated—a high-capacity, size and charge-selective route (pore pathway) and a low-capacity, nonselective route (leak pathway). Only small molecules can pass through the pore pathway (less than ~7 Å diameter), while larger molecules such as lipopolysaccharides can pass via the leak pathway (<~100 Å diameter) (19). A third tight junction-independent unrestricted pathway, which does not have a size limit, occurs at sites of epithelial damage. Other than direct cellular invasion and transcytosis, this is the only route by which intact bacteria can cross the epithelial barrier (10).

Author contributions: T.O., S.A., T.S., J.R.T., and C.M.C. designed research; T.O., S.A., T.S., Y.Y.S., Z.L., E.M.B., and S.T. performed research; T.O., S.A., T.S., C.-W.C., Y.Y.S., Z.L., E.M.B., A.B.F., J.T.R., S.T., M.L.F., J.R.T., and C.M.C. analyzed data; and T.O., S.A., J.R.T., and C.M.C. wrote the paper.

The authors declare no competing interest.

This article is a PNAS Direct Submission. T.R.B. is a guest editor invited by the Editorial Board.

[1]T.O. and S.A. contributed equally to this work.

[2]To whom correspondence may be addressed. Email: jrturner@bwh.harvard.edu or cmcoop3@emory.edu.

This article contains supporting information online at https://www.pnas.org/lookup/suppl/doi:10.1073/pnas.2217877121/-/DCSupplemental.

Published February 27, 2024.

The claudin family of tight junction proteins defines both pore pathway permeability and barrier function, depending on which of the 27 different claudin genes are expressed (13, 20, 21). Claudin-2 is a prototypical pore-forming molecule that, in the gut, is downregulated after weaning but upregulated during inflammatory states. Claudin-2 forms channels that accommodate water, and Na^+ but exclude larger molecules (22). In vitro, IL-6, IL-13, IL-22, and, possibly, tumor necrosis factor (TNF), activate claudin-2 transcription and protein expression (23–26). In vivo, IL-13- or IL-22-induced claudin-2 expression increases paracellular flux of small cations (12). Mice lacking claudin-2 develop normally (27–29), but are protected from IL-13-induced permeability increases while, conversely, transgenic claudin-2 overexpression similarly enhances paracellular cation flux without cytokine stimulation (12). Claudin-2 is, therefore, necessary for cytokine-induced upregulation of pore pathway permeability and is sufficient to effect similar permeability increases without cytokine stimulation (12).

Both claudin-2 KO and claudin-2 transgenic mice grow and gain weight normally (12, 23, 29–31), which prompts the question of why intestinal epithelial claudin-2 is expressed at high levels prior to weaning and in disease. Studies of claudin-2 KO and transgenic mice have shown that increased expression reduces severity and promotes resolution of *Citrobacter rodentium* colitis (23). This is, at least partially, a consequence of water efflux into the gut lumen via claudin-2 channels (23). Water efflux and consequent dilution of dextran sulfate sodium (DSS) may also explain the resistance of claudin-2 transgenic mice to chemical colitis (32) although recent work suggests that claudin-2 may also contribute to mucosal healing (31). Conversely, immune-mediated experimental inflammatory bowel disease is attenuated in claudin-2 KO mice and exacerbated by transgenic claudin-2 overexpression (12) suggesting that claudin-2 upregulation may enhance immune activation.

Intestinal epithelial claudin-2 expression is elevated following sepsis induced by cecal ligation and puncture (CLP), a pre-clinical model of intraabdominal sepsis, as well as *Pseudomonas aeruginosa* pneumonia (11, 33–36). However, the functional significance of claudin-2 upregulation in sepsis is undefined.

Here, we examined resection specimens from septic and non-septic patients and found that, as in mice, intestinal epithelial claudin-2 expression is upregulated in septic patients. Studies in claudin-2 KO and WT mice showed that claudin-2 upregulation is associated with sepsis-associated increases in paracellular pore pathway permeability, dysbiosis, mucosal and systemic inflammation, intestinal damage, and mortality. Pharmacological targeting of claudin-2 function may, therefore, have potential as a therapeutic intervention in sepsis.

Results

Intestinal Claudin-2 Protein Expression Is Selectively Upregulated in Septic Patients. Many studies have characterized the intestinal barrier loss that occurs in experimental bowel perforation–induced sepsis via the CLP model, and some have examined transcription and expression of a limited number of tight junction-associated proteins (11, 33, 36–39). Although similar increases in intestinal permeability occur in septic patients (40), no detailed analyses have been reported. We performed quantitative multiplex immunofluorescence analysis of ileal tissues from 27 patients with sepsis due to intestinal perforation (all with Sequential Organ Failure Assessment, i.e., SOFA, scores ≥2, consistent with Sepsis 3 definition) and 56 age- and sex-matched control patients who underwent elective intestinal resection (Table 1). The greatest number of sepsis cases were secondary to appendiceal perforation. In order to avoid focal changes due to perforation-adjacent inflammation and severe serositis, ileal tissues studied were at least 5 cm from the perforation site and had, at most, mild active serositis (Fig. 1*A*). Mucosal immune cell infiltrates were markedly increased in septic patients, with the largest changes in neutrophil and macrophage numbers (Fig. 1 *A* and *B*). Total numbers of $CD3^+$ and $CD8^+$ T cells within the mucosa were not changed (*SI Appendix*, Fig. S1). Within the epithelium, the number of Ki67-positive proliferating crypt cells was modestly reduced in septic patients (Fig. 1*C*). More striking, however, was the dramatically increased claudin-2 expression, particularly within the crypt epithelium in septic patients (Fig. 1*D*). Conversely, expression of claudin-15, the other claudin that forms cation-selective pores within intestinal epithelial tight junctions, was modestly reduced in sepsis. In contrast to claudins 2 and 15, expression of claudins 3, 4, and 7, JAM-A, occludin, ZO-1, and E-cadherin were unaffected by sepsis (*SI Appendix*, Fig. S1).

Table 1. Clinical characteristics of septic patients and controls

	Septic patients (SOFA ≥ 2) (n = 27)	Non-septic controls (n = 56)
Age (mean, range)	61 y (26 to 81)	58 (26 to 91)
Gender (M:F)	58%:42% (n = 16:11)	51% (n = 29)
Blood culture	Gram (−) anaerobes: 37% (n = 10) Candida: 7% (n = 2)	NA
SOFA score	4.1 (2 to 9)*	NA
Cause of perforation	Appendicitis: 33% (n = 9) Ischemia: 15% (n = 4) Neoplastic disease: 7.5% (n = 2) Diverticulitis: 7.5% (n = 2) Obstruction: 7.5% (n = 2) Hernia: 7.5% (n = 2) Unknown: 22% (n = 6)	Nonperforated neoplastic disease: 100% (n = 56)
Site of perforation	Ileum: 11% (n = 3) Appendix: 33% (n = 9) Right colon: 48% (n = 13) Left colon: 8% (n = 2)	NA
Procedure	Ileocecectomy: 56% (n = 15) Right hemicolectomy: 33% (n = 9) Total colectomy: 11% (n = 3)	Ileocecectomy: 5% (n = 3) Right hemicolectomy: 75% (n = 43) Total colectomy: 18% (n = 10) Small bowel resection: 2% (n = 1)

*SOFA scores shown are based on available information, which was inadequate to score all organ systems. Thus, the actual SOFA scores are greater than those listed above.

Abdominal Sepsis in Mice Induces Changes that Recapitulate Human Bowel Perforation. We next sought to determine whether the mouse CLP model of bowel perforation and sepsis induced changes similar to those observed in human disease. Histologically, CLP tissue demonstrated increased numbers of lamina propria and intraepithelial neutrophils, a general increase in lamina propria cellularity, and reduced epithelial proliferation (Fig. 2 *A* and *C*). Although gross epithelial damage, such as ulceration, was not present, pore pathway permeability, measured as the ratio of creatinine to 70-kDa dextran recovery, was markedly increased after CLP (Fig. 2*B*).

Pore pathway permeability reflects flux across paracellular channels formed by claudins (19, 22, 41). Thus, mRNA encoding claudin proteins were assessed by qRT-PCR (*SI Appendix*, Fig. S2*A*). Consistent with previously published work (11), claudin-2 mRNA was significantly increased in tissue from CLP mice relative to those that underwent sham surgeries (*SI Appendix*, Fig. S2*A*). mRNA species encoding claudins 5, 8, and 13 were also increased after CLP (*SI Appendix*, Fig. S2*A*). Notably, claudin-5 expression is primarily expressed in vascular endothelial

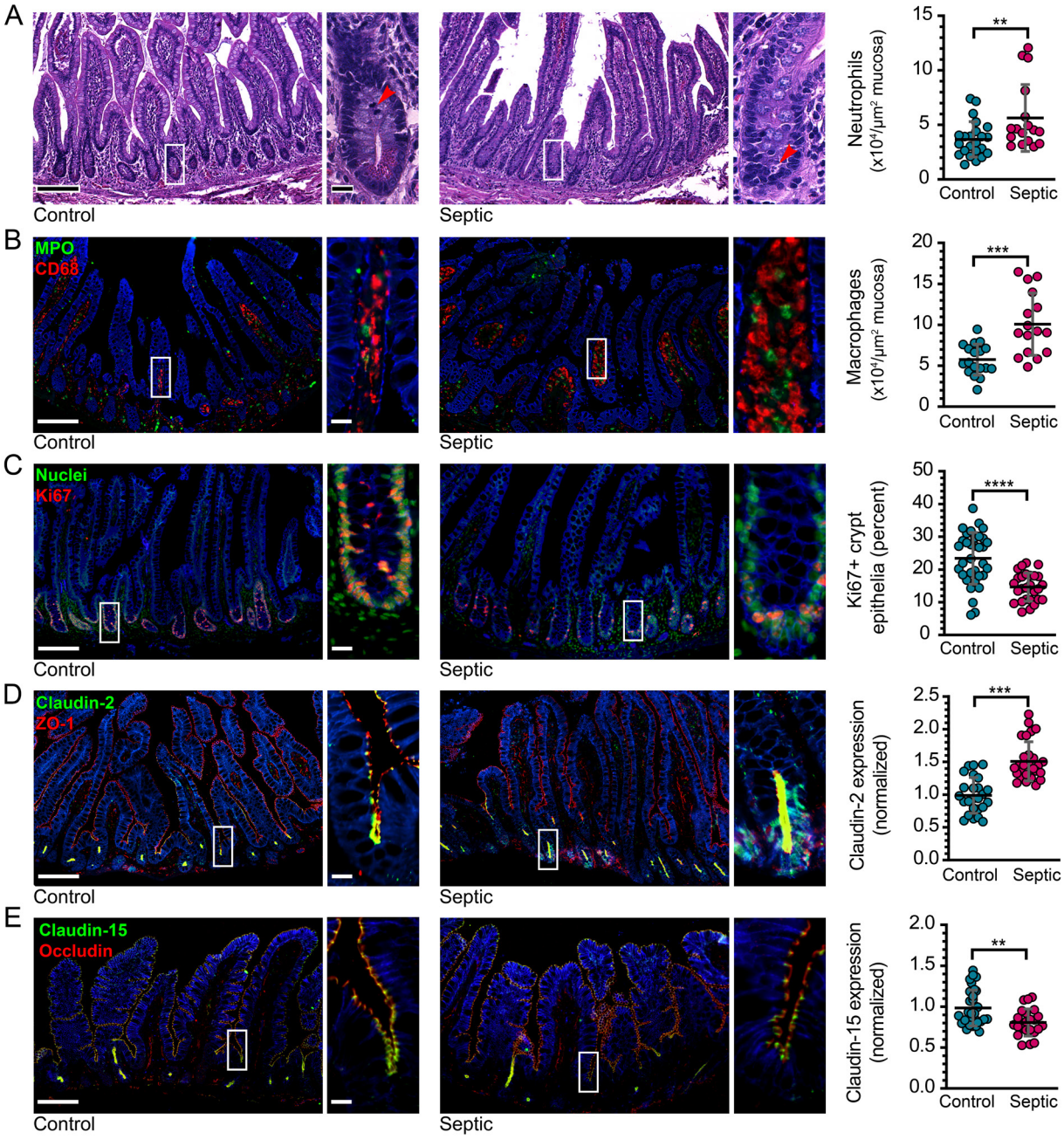

Fig. 1. Tight junction protein expression is modified in septic patients. (*A*) Representative histopathology of ileal tissue from a control subject (*Left*) and a septic patient (*Right*). Note the mitosis in the control and apoptotic body in the septic conditions (arrows). (*B*) Representative immunofluorescent staining of myeloperoxidase-positive neutrophils (green) and CD68-positive macrophages (red). The graphs show numbers of neutrophils and macrophages within mucosa of control subjects (cyan) and septic patients (magenta). (*C*) Ki67 (red) staining shows proliferating cells. Nuclear stain (Hoechst 33258, green) is shown for reference. (*D*) Claudin-2 (green) expression is increased in sepsis. ZO-1 (red) is unchanged and shown for reference. (*E*) Claudin-15 (green) expression is reduced in sepsis. Occludin (red) is unhanged and shown for reference. n = 57 healthy controls (23 for macrophages) and 27 septic patients. Each point represents a unique subject/patient. *$P < 0.05$; **$P < 0.01$; ***$P < 0.001$. NaK ATPase (blue) is shown for reference in panels (*B*–*E*). Scale bars, 100 µm and 20 µm (*Insets*).

cells (42, 43) and is unlikely to reflect changes in epithelial barrier function. Claudin 13 is not expressed in humans (44).

In order to determine whether mRNA increases reflected changes in protein expression, morphometric analysis was performed on jejunal sections from mice that underwent sham surgery or CLP. Consistent with the qRT-PCR data of mouse tissues and the morphometry of human tissues, jejunal (Fig. 2*D*) and colonic (Fig. 2*G*) epithelial claudin-2 expression was dramatically increased after CLP. Although claudin-15 mRNA was unchanged, claudin-15 protein expression was decreased after CLP, similar to the changes observed in human sepsis (Fig. 2*E*). Consistent with the mRNA data, claudin-4 expression was unchanged (Fig. 2*F*). Claudin-5 epithelial expression was not different between sham and CLP and was primarily restricted to endothelial cells (*SI Appendix*, Fig. S2 *B* and *C*).

Claudin-2 Deletion Attenuates CLP-Induced Increases in Pore and Unrestricted Pathway Permeabilities. Upregulation of claudin-2, a prototypical pore-forming claudin, may explain the increased creatinine to 70-kDa dextran recovery ratio after CLP. To test this hypothesis, we analyzed pore, leak, and unrestricted pathway permeabilities in WT and claudin-2 KO mice following CLP using a three-probe assay that allows independent analysis

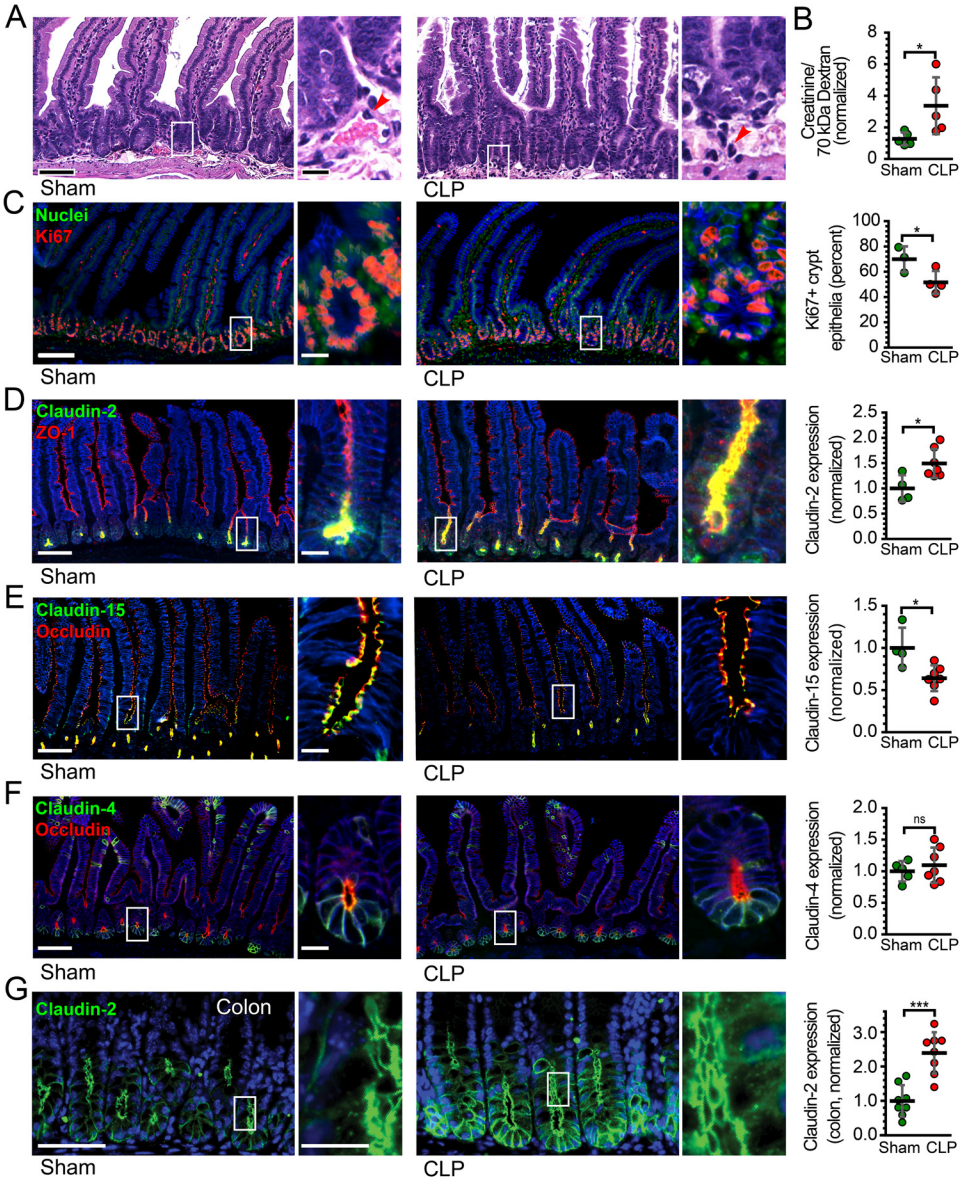

Fig. 2. Tight junction protein expression changes after CLP recapitulate human sepsis. (*A*) Representative histopathology of jejunal tissue from a sham control (*Left*) and CLP (*Right*) mouse. (*B*) Pore pathway permeability, measured as the ratio of creatinine to 70-kDa dextran recovery, at 12 h after sham or CLP. Sham controls (green) and CLP (red) mice are shown. (*C*) Ki67 (red) staining of jejunal tissue shows proliferating cells. Nuclear stain (Hoechst 33258, green) is shown for reference. (*D*) Claudin-2 (green) expression is increased in jejunal enterocytes after CLP. ZO-1 (red) is unhanged and shown for reference. (*E*) Claudin-15 (green) expression is reduced in jejunal enterocytes after CLP. Occludin (red) is unhanged and shown for reference. (*F*) Neither claudin-4 (green) nor occludin (red) expression are changed after CLP. (*G*) Colonic claudin-2 expression is upregulated after CLP. n = 3 to 8 for each condition. Each point represents a unique mouse. $*P < 0.05$; $**P < 0.01$; $***P < 0.001$. NaK ATPase (blue) is shown for reference in panels (*C*–*G*). Scale bars, 100 μm and 20 μm (*Insets*).

of pore pathway, leak, and unrestricted pathways in vivo (Fig. 3*A*) (23, 45).

Creatinine permeability, indicative of pore pathway flux, was significantly increased in WT, but not claudin-2 KO, mice within 12 h of CLP (Fig. 3*B*). More importantly, 4-kDa dextran (Fig. 3*C*) and 70-kDa dextran (Fig. 3*D*) permeabilities were markedly increased in WT mice at 12 and 24 h after CLP. In contrast, 4-kDa dextran permeability was modestly increased, and maximal 70-kDa dextran permeability increases of 1.4-fold in claudin-2 KO mice were far less than the 6.3-fold increases observed in WT mice. Taken together, the permeability data indicate that, beginning at 24 h after CLP, increased creatinine, 4-kDa dextran, and 70-kDa dextran permeabilities seen in WT mice are secondary to increased unrestricted pathway permeability secondary to epithelial damage. In contrast, the increased permeabilities of creatinine and 4-kDa dextran in WT mice, and of 4-kDa dextran in claudin-2 KO mice, at 12 h after CLP reflect increased pore and leak pathway flux, respectively. Claudin-2 deletion therefore prevents CLP-induced increases in intestinal pore pathway permeability.

Expression of claudins 3 and 7 as well as JAM-A within epithelial cells was unaffected by CLP in either WT or claudin-2 KO mice (*SI Appendix*, Fig. S3). The leak pathway permeability increases that occurred at 12 h after CLP cannot, therefore, reflect altered expression of these proteins. We therefore assessed cytoskeletal regulation downstream of myosin light chain kinase activation, the most common cause of pathophysiologic leak pathway barrier loss (13, 46–48). Consistent with the permeability data, MLC phosphorylation was significantly increased in both WT and claudin-2 KO mice following a septic insult, but, when the two genotypes were compared, these increases were not significantly different (*SI Appendix*, Fig. S4*A*). Therefore, although claudin-2 KO blocks CLP-induced increases in pore pathway flux and markedly delays unrestricted pathway permeability increases, it does not prevent leak pathway upregulation.

Claudin-2 Promotes Tissue Damage after CLP. The 70-kDa dextran permeability data showing that claudin-2 KO mice are relatively protected from increases in unrestricted pathway permeability after CLP indicate that claudin-2 deletion attenuates epithelial damage. To better understand the underlying mechanisms, we first assessed histopathology of WT and claudin-2 KO mice after sham surgery or CLP. Histopathological injury scores were significantly increased in WT mice after CLP and were far greater than the modest increases observed in claudin-2 KO mice (Fig. 3*E*). Gross

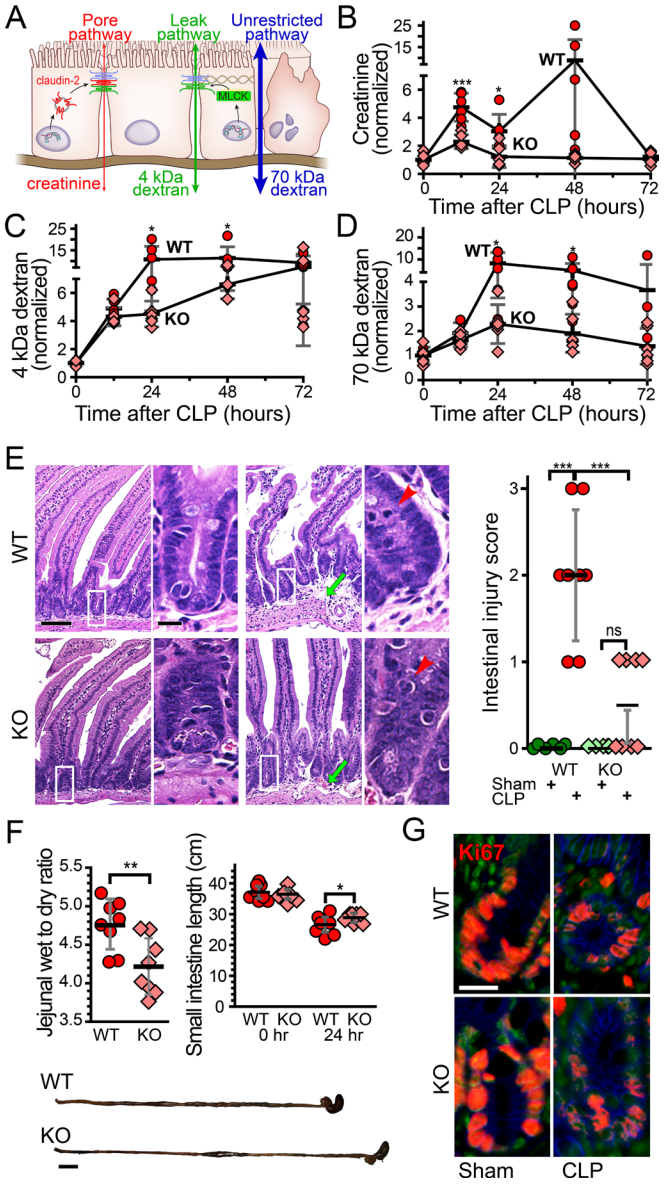

Fig. 3. CLP causes claudin-2-dependent increases in pore pathway permeability and limits epithelial damage (unrestricted pathway) flux. (*A*) Paracellular flux across tight junctions is mediated by two distinct routes, pore and leak pathways, which can be measured by creatinine (6 Å diameter) and 4-kDa dextran (28 Å diameter) flux, respectively. Permeability of the nonselective unrestricted pathway is assessed using 70-kDa dextran (120 Å diameter). (*B*) Creatinine flux (pore pathway permeability) increases 12 h after CLP in WT (red), but not claudin-2 KO (pink), mice. (*C*) 4-kDa dextran flux (leak pathway permeability) is greater in both WT and claudin-2 KO mice at 12 h after CLP. 4-kDa dextran permeability increases further at 24 h. (*D*) Permeability of the epithelial damage-dependent unrestricted pathway increases in WT, but not claudin-2 KO, mice within 24 h after CLP. (*E*) Representative jejunal histopathology of WT or claudin-2 KO mice 12 h after sham or CLP. The degree of submucosal edema (green arrows) and intraepithelial neutrophil infiltration (red arrows) in WT mice is greater than in claudin-2 KO mice. Scale bar, 50 μm. (*F*) Jejunal edema and inflammation, measured as wet to dry ratio, is significantly higher in WT, relative to claudin-2 KO, mice at 24 h after CLP. This correlates with a greater degree of small intestinal shortening after CLP in WT, relative to claudin-2 KO, mice. Scale bar, 1 cm. (*G*) CLP causes similar decreases in numbers of Ki67+ proliferating cells (red) within WT and claudin-2 KO mice at 12 h. Nuclei (Hoechst 33258, green) and NaK ATPase (blue) are shown for reference. n = 6 to 8 for each genotype at each time point. Scale bar, 20 μm. *$P < 0.05$; **$P < 0.01$; ***$P < 0.001$.

pathology was also significantly different between the genotypes, with less edema, as indicated by tissue weight to dry ratio, and small intestinal shortening in claudin-2 KO mice (Fig. 3*F*). To explain the gross histologic differences between the genotypes, we considered the possibility that epithelial proliferation and repair might differ. Numbers of Ki67$^+$ crypt epithelial cells were, however, similarly reduced after CLP in both WT and claudin-2 KO mice (Fig. 3*G* and *SI Appendix*, Fig. S4*C*). Similarly, numbers of crypt and transit-amplifying epithelial cells synthesizing DNA, as detected by BrdU labeling (*SI Appendix*, Fig. S4*D*), and apoptotic cells as measured by cleaved caspase-3 positive crypt cells (*SI Appendix*, Fig. S4*E*) were similar in WT and claudin-2 KO mice.

Claudin-2 Expression Leads to Mucosal Immune Activation. Immune activation often leads to tissue damage in sepsis. We therefore asked whether recruitment of immune cells to the mucosa was affected by claudin-2 expression. Quantitative morphometry confirmed marked increases in mucosal macrophages and neutrophils after CLP, similar to that seen in septic patients (Fig. 4*A*). These increases were, however, comparable in WT and claudin-2 KO mice (Fig. 4*A*). We also assessed T cell numbers throughout the mucosa (Fig. 4*B*) and within the intraepithelial compartment (*SI Appendix*, Fig. S5*A*). These were not affected at 24 h after CLP. Moreover, numbers of CD4$^+$ or CD8$^+$ T cells within the mucosa or epithelium, respectively, were unaltered (Fig. 4*B* and *SI Appendix*, Fig. S5*A*).

We next asked whether T cell subset populations after CLP were altered by claudin-2 KO mice. Among intraepithelial lymphocytes (IELs), there were significantly fewer CD3$^+$CD8αβ T cells in septic claudin-2 KO mice although there were no differences in numbers of TCRγδ$^+$ and TCRγδ$^-$ IELs (Fig. 4*C*). Analyses of cytokine expression within T cell subsets revealed significantly fewer IL-17-producing cells among both TCRγδ$^+$ and TCRγδ$^-$ IELs in septic claudin-2 KO mice (Fig. 4*D* and *SI Appendix*, Fig. S5*C*). The intraepithelial compartment of septic claudin-2 KO mice also had fewer numbers of TNF-producing IELs, which was primarily due to differences among CD8α$^+$CD8β$^-$ T cells (*SI Appendix*, Fig. S5*B*).

Although quantitative immunohistochemistry failed to show differences in bulk T cell numbers, IL-1β and IL-6 expression within mucosal homogenates were reduced in septic claudin-2 KO, relative to WT, mice; mucosal IL-10, IL-13, TGFβ2, IL-22, and IFNγ were similar in both genotypes (Fig. 4*E* and *SI Appendix*, Fig. S5*B*).

Within Peyer's patches, septic claudin-2 KO mice had significantly fewer activated CD4$^+$CD69$^+$ T cells than WT mice (Fig. 4*F*). Consistent with decreased activation, claudin-2 KO mice also demonstrated decreased numbers of Peyer's patches CD4$^+$CD25$^+$ T cells and CD8$^+$CD25$^+$ T cells relative to WT mice (Fig. 4*F*). The fractions of CD44^{high} and CD62L^{low} T cells within Peyer's patch were, however, similar in WT and claudin-2 KO mice (*SI Appendix*, Fig. S5*D*), as were serum cytokine levels (*SI Appendix*, Fig. S5*E*). As a whole, these data indicate that claudin-2 expression leads to increased T cell activation in sepsis with limited changes in pro-inflammatory cytokine production.

Intestinal Epithelial Claudin-2 Exacerbates Sepsis-Induced Peritonitis. We considered the possibility that loss of claudin-2 expression within renal proximal tubules or hepatocytes could affect CLP-associated renal or hepatic damage, respectively, and interfere with CLP-induced immune responses. However, CLP did not affect renal (Fig. 5*A*) or hepatocellular (Fig. 5*B*) claudin-2 expression. Moreover, neither serum creatinine and renal histology (Fig. 5*C*) nor serum aspartate aminotransferase (AST) and liver histology (Fig. 5*D*) were affected by sepsis in WT or claudin-2 KO mice, as was lung histology (not shown). In contrast, intestinal tissue injury was reduced in claudin-2 KO mice relative to WT mice (Fig. 3*E*). These data suggest that, despite use of a global claudin-2 KO mice in these studies, intestinal epithelial cells are

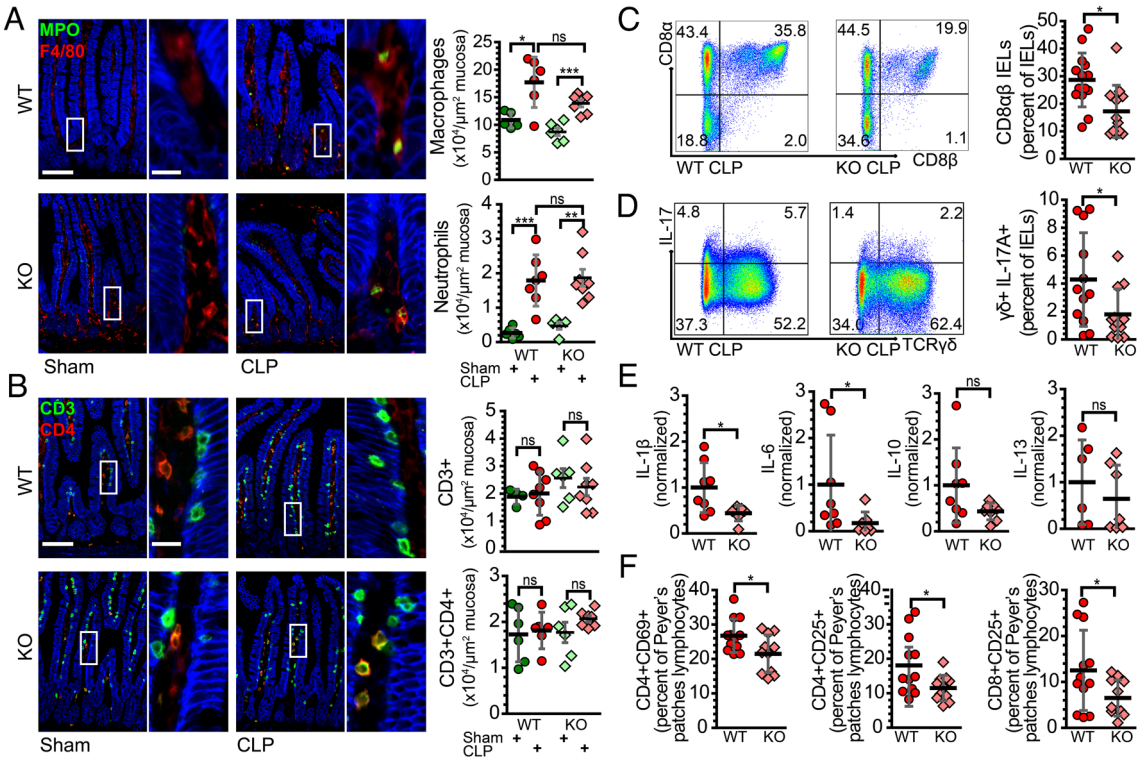

Fig. 4. Claudin-2 expression augments mucosal immune activation. (*A*) Representative immunofluorescent staining of myeloperoxidase-positive neutrophils (green) and F4/80-positive macrophages (red). The graphs show numbers of neutrophils and macrophages within mucosa of sham WT (green) and claudin-2 KO (light green) and CLP WT (red) and claudin-2 KO (pink) mice. (*B*) Mucosal CD3+CD4- (green) and CD3+CD4+ (yellow) T cell infiltration is similar across all conditions. (*C*) Flow cytometric plot and graph of CD8αβ IEL numbers 24 h after CLP. (*D*) Flow cytometric plot and graph of IL-17 producing TCRγδ IELs after CLP. (*E*) Cytokine mRNA expression shows that claudin-2 KO mice have reduced IL-1β and IL-6 transcription, relative to WT, at 24 h after CLP. (*F*) Within Peyer's patches, the fractions of CD4+CD69+, CD4+CD25+, and CD8+CD25+ lymphocytes among all CD3+ cells were significantly greater in WT, relative to claudin-2 KO, mice. n = 5 to 12 for each condition. **P* < 0.05; ***P* < 0.01; ****P* < 0.001. NaK ATPase (blue) is shown for reference (*A* and *B*). Scale bars, 100 µm, 20 µm (*Insets*).

the primary site at which claudin-2 loss attenuates CLP-induced disease.

We next focused on the peritoneal cavity. Peritoneal fluid IL-10 was lower in claudin-2 KO mice, but IL-6 levels were similar (Fig. 5*E*). Numbers of peritoneal neutrophils, macrophages, and dendritic cells were also significantly lower in claudin-2 KO mice than in WT mice (Fig. 5 *F* and *G*). These changes correlated with a decreased bacterial burden in the peritoneal fluid (but not the blood) of claudin-2 KO mice 48 h after the onset of sepsis (Fig. 5*H*). Most importantly, CLP-induced weight loss was limited (Fig. 5*I*) and survival was markedly increased (Fig. 5*J*) by claudin-2 KO.

Claudin-2 Promotes Sepsis-Associated Dysbiosis. Intestinal microbiome alterations are implicated as modifiers of sepsis morbidity and mortality (16, 49–55). We therefore asked whether claudin-2 might also impact the gut microbiome and whether this could contribute to the effects of claudin-2 on sepsis severity. Under baseline conditions, global microbiome composition differed modestly between WT and claudin-2KO mice despite their being raised in the same facility (Fig. 6*A*). However, relative abundances of *Bacteroidetes* and *Firmicute spp.* (Fig. 6 *B* and *C*) were similar in both genotypes. To examine the impact of claudin-2 on the microbiome after sepsis, the identical analysis was performed following CLP. The microbiota of both WT and claudin-2 KO mice changed significantly within 24 h of CLP (Fig. 6*A*). *Firmicute spp.* abundances were increased in both claudin-2 KO and WT mice, but to a significantly greater degree in KO mice (Fig. 6*B*). Conversely, *Bacteroidetes* abundances were reduced after CLP, and these changes were similar in the two genotypes (Fig. 6*C*). Thus, claudin-2 may modestly alter the microbiome under basal conditions but has substantial effects on development of sepsis-associated dysbiosis.

We next asked whether the distinct microbiome shifts induced by CLP in WT or claudin-2 KO mice might affect sepsis severity. Cecal contents were collected from WT or claudin-2 KO mice 24 h after CLP. A slurry of cecal contents was then delivered to healthy WT mice by intraperitoneal injection (Fig. 6*D*). Survival of WT mice injected with claudin-2 KO CLP slurry was far greater than that of WT mice injected with WT CLP slurry (Fig. 6*E*). In contrast, survival was 100% in both WT mice injected with heat-inactivated claudin-2 KO CLP slurry and WT mice injected with heat-inactivated WT CLP slurry (n = 16 for both, *SI Appendix*, Fig. S6). Thus, the impact of claudin-2 effects on sepsis-induced microbiome alterations contributes to the enhanced survival of claudin-2 KO mice after CLP.

CK2 (Casein Kinase 2) Inhibition Does Not Prevent Sepsis-Induced Dysbiosis. We previously showed that CK2 inhibition can inactivate claudin-2 channels in vitro and in vivo (12, 56). Moreover, we previously showed that oral delivery of a systemic CK2 inhibitor, silmitasertib (CX-4945), attenuates severity of experimental immune-mediated colitis and that this effect requires the presence of claudin-2. We, therefore, treated mice with silmitasertib either prior to CLP or following CLP. Microbiota of vehicle and silmitasertib-treated mice were similar to one another before CLP. Moreover, silmitasertib did not affect CLP-induced dysbiosis (*SI Appendix*, Fig. S7). Additionally, no difference in mortality was detected in mice given silmitasertib or vehicle (*SI Appendix*, Fig. S7). Thus, the effect of claudin-2 deletion on microbial response to sepsis cannot be reproduced by systemic CK2 inhibition.

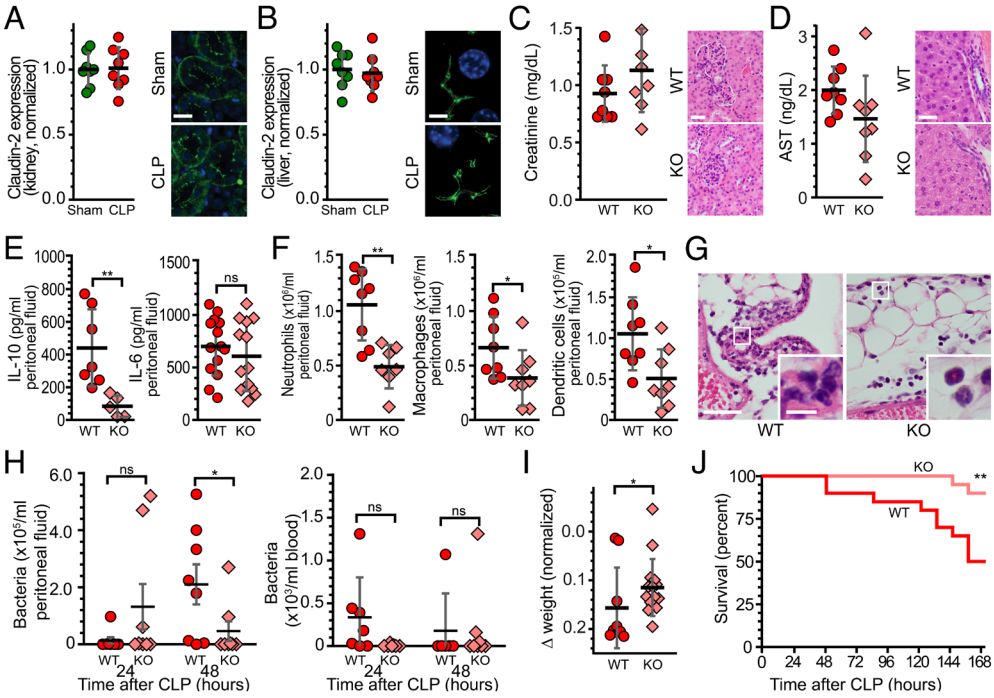

Fig. 5. Intestinal epithelial claudin-2 expression exacerbates peritonitis and increases mortality after CLP. (*A*) Renal tubular claudin-2 expression is not affected by CLP. n = 8 sham and 8 CLP mice. Scale bar, 20 μm. (*B*) Hepatocellular claudin-2 expression is not affected by CLP. n = 8 sham and 8 CLP mice. Scale bar, 5 μm. (*C*) Serum creatinine and renal histology of WT and claudin-2 KO mice at 24 h after CLP. Scale bar, 50 μm. (*D*) Serum AST and liver histology of WT and claudin-2 KO mice at 24 h after CLP. Alanine aminotransferase (ALT) was below detection limits in all mice. (Scale bar, 20 μm.) (*E*) The peritoneal fluid of WT mice (red) contains significantly more IL-10 than that of claudin-2 KO mice (pink) at 24 h after CLP. (*F*) Numbers of neutrophils, macrophages, and dendritic cells were significantly greater in peritoneal fluid of WT (n = 8), relative to claudin-2 KO (n = 8), mice at 24 h after CLP. (*G*) Representative histology showing greater neutrophilic infiltration of subserosal adipose tissue and more extensive peritonitis in WT, relative to claudin-2 KO, mice. Scale bars, 100 μm, 20 μm (*Insets*). (*H*) Bacteremia was not different between groups. (*I*) CLP-induced weight loss did not occur in claudin-2 KO mice. (*J*) Claudin-2 KO mice displayed 90% survival at 168 h (7 d) after CLP relative to only 50% survival of WT mice. n = 20/both WT and KO in the survival curve. $*P < 0.05$; $**P < 0.01$; $***P < 0.001$.

Discussion

This study demonstrates that claudin 2 is upregulated in the intestinal epithelium of septic patients compared to those who undergo elective bowel resection and defines the impact of claudin-2 upregulation using the pre-clinical CLP model of sepsis and claudin-2 KO mice. The data indicate that the epithelial claudin-2 upregulation induced by sepsis leads to increased pore pathway permeability that is associated with dysbiosis, immune activation, augmented epithelial damage and increased mortality. Conversely, inflammation, intestinal damage, and peritoneal cavity bacterial burden are all reduced in claudin-2 KO mice, which also display distinct microbiome changes and, most importantly, increased survival relative to WT mice.

This study overcomes the inherent technical challenges and assesses intestinal epithelial expression of tight junction proteins in a large cohort of septic patients. Previous work has shown that claudin-2 mRNA is elevated in the blood of septic patients, but has not identified the cellular source of this claudin-2 mRNA (57). Our data document increased ileal epithelial claudin-2 expression in patients undergoing resections for sepsis relative to those whose resections were for other indications. In selecting patients and tissues for analysis, we excluded pediatric patients, as claudin-2 expression is much greater in children than adults (58). Moreover, all samples were from sites well-separated from serositis in order to avoid confounding effects of local inflammation. Nevertheless, it is important to recognize that while the mouse antibiotic regimen was standardized in our experiments, septic patients assuredly received a variety of different antibiotic regimens whereas control patients may not have received antibiotics at all. This likely leads to different antibiotic-associated differences in the microbiome between mice and humans over and above pre-existing differences between homogenous mice in a barrier facility and genetically diverse humans within different environments. Further, while we have included all available information about surgical patients, age, sex, culture results, organ dysfunction, cause and site of perforation and operation performed varied. In addition, it is a certainty that there must be variation in (at a minimum) co-morbidities, weight loss and/or malnutrition prior to surgery, dysbiosis, vasopressor exposure, and mechanical bowel preparation, each of which could impact claudin-2 expression. Additionally, there is an inherent selection bias in the patient groups, as the samples came from resections that, by definition, included the ileum. We cannot know what specimens would look like in patients who underwent surgery for similar indications but did not have an ileal resection. Thus, although the concordance between these human data and those from mice after CLP is remarkable, statistical analysis of claudin-2 expression and its correlation with clinical parameters in septic patients will require further study.

Our data agree with previous work showing increased *CLDN2* mRNA in peripheral blood of sepsis patients (57), but are discordant with one previous study that failed to detect altered claudin-2 expression in colectomy specimens from critically ill patients (59). Possible explanations for this include analysis of ileum versus colon, although we showed that, in mice, colonic claudin-2 upregulation parallels that seen in the small intestine. Alternatively, the antibody used for claudin-2 detection could explain the discordance. Specificity problems plague commercially available claudin-2 antibodies, and the antibody used in the previous study was not specified and no images were shown. In contrast, we generated our own affinity-purified rabbit anti-claudin-2 polyclonal antibodies and validated their specificity using claudin-2 KO mouse

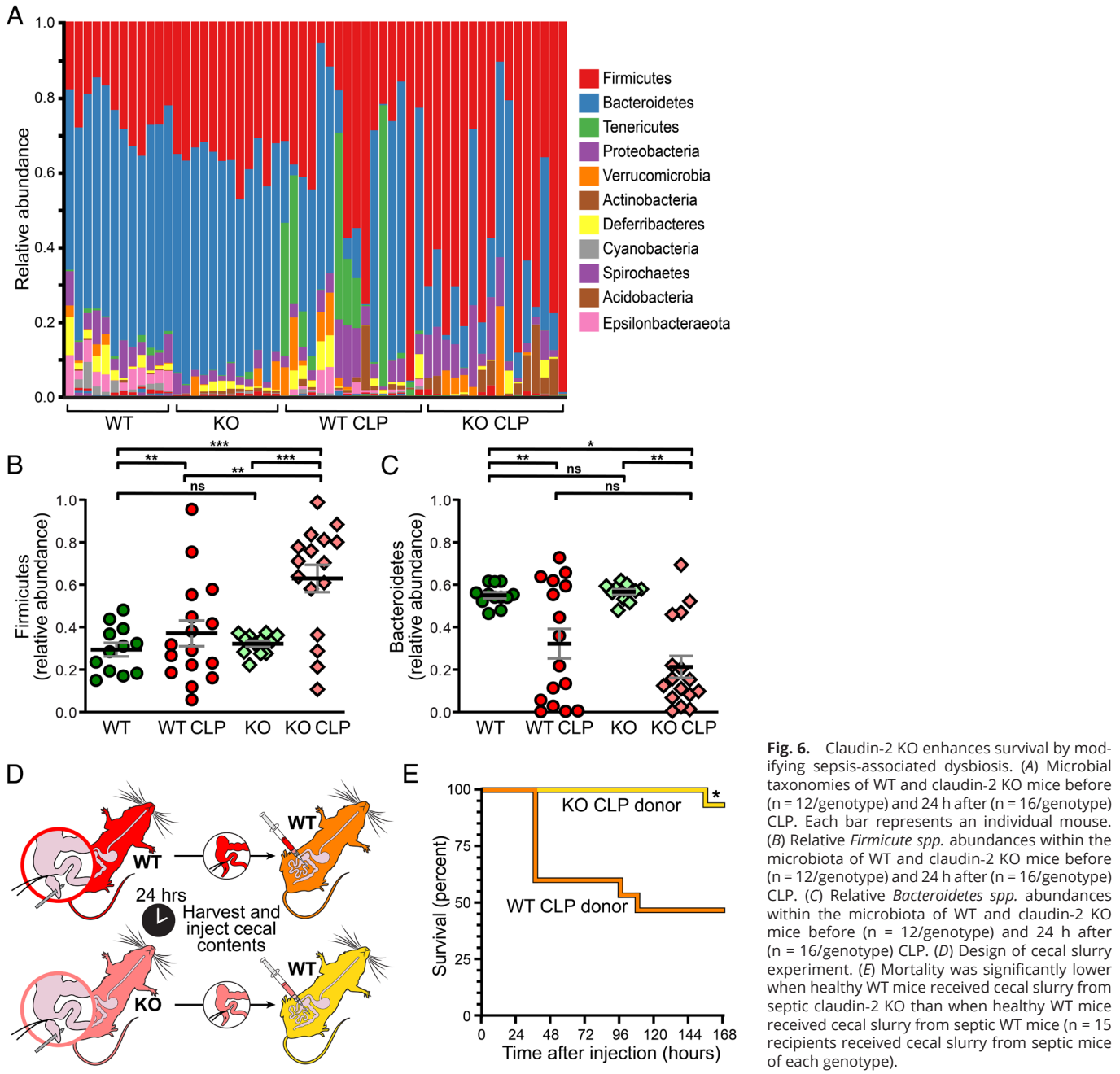

Fig. 6. Claudin-2 KO enhances survival by modifying sepsis-associated dysbiosis. (*A*) Microbial taxonomies of WT and claudin-2 KO mice before (n = 12/genotype) and 24 h after (n = 16/genotype) CLP. Each bar represents an individual mouse. (*B*) Relative *Firmicute spp.* abundances within the microbiota of WT and claudin-2 KO mice before (n = 12/genotype) and 24 h after (n = 16/genotype) CLP. (*C*) Relative *Bacteroidetes spp.* abundances within the microbiota of WT and claudin-2 KO mice before (n = 12/genotype) and 24 h after (n = 16/genotype) CLP. (*D*) Design of cecal slurry experiment. (*E*) Mortality was significantly lower when healthy WT mice received cecal slurry from septic claudin-2 KO than when healthy WT mice received cecal slurry from septic WT mice (n = 15 recipients received cecal slurry from septic mice of each genotype).

tissue as well as a claudin-2 KO human intestinal epithelial cell line (Table 2).

A key first step was to replicate prior work demonstrating that claudin-2 mRNA and protein are elevated following sepsis in mice (11, 33, 60). After determining that intestinal claudin-2 expression was upregulated following CLP, we sought to identify the mechanisms of associated intestinal permeability changes using specific probes for the tight junction pore and leak pathways as well as the tight junction-independent unrestricted pathway. These data emphasize the multifactorial nature of intestinal barrier loss in sepsis, as CLP increases flux across all three pathways. However, the kinetics as well as the effect of claudin-2 deletion on each pathway are distinct. Claudin-2 KO mice are specifically protected from early increases in pore pathway permeability and display delay and attenuation of 70-kDa dextran permeability increases relative to WT mice. The latter result could be misinterpreted as indicating that claudin-2 mediates flux of dextrans, as has been stated previously (61). However, many in vitro and in vivo studies have carefully analyzed the size selectivity of claudin-2 channels and definitively demonstrated that they cannot accommodate dextrans or any molecules with diameters greater than ~7 Å (12, 22, 28, 62). It is therefore more likely that claudin-2 expression enhances disease progression and associated epithelial damage, as has been shown in immune-mediated colitis (12). For example, similar to occludin (63), claudin-2 upregulation in sepsis expression might promote epithelial apoptosis (64–66). Although we did not detect epithelial apoptosis differences between WT and claudin-2 KO mice, the rapid extrusion of apoptotic and damaged epithelial cells may have interfered with their detection in histologic sections (Table 3).

Claudin-2 mediated paracellular Na^+ and water flux could, potentially, affect mucosal immune activation by unknown mechanisms, as has been observed in experimental inflammatory bowel disease (12). Alternatively, claudin-2 deletion may limit Na^+-dependent active transport and, secondarily, reduce absorption of microbial products, such as formylated bacterial di- and tri-peptides via the

H+-coupled peptide transporter pepT1 (67). However, due to their exquisite size-selectivity, paracellular flux of such peptides, bacterial metabolites, or other substances across claudin-2 channels is not a serious consideration.

Claudin-2-mediated paracellular Na^+ and water flux might be expected to expand or collapse lateral intercellular spaces, depending on the direction of movement. This could be consistent with the reduced numbers of CD8αβ T cells and IL-17-producing lymphocytes within lateral intercellular spaces, i.e., IELs. This observation in mice is similar to the reported association between increased numbers of Th17 cells, greater disease severity, and worse prognosis in septic patients (68) as well as a report that microRNA that reduces Th17 differentiation and enhances Treg differentiation improved survival in septic rats (69). In addition, expression of the sepsis-associated pro-inflammatory cytokines IL-1β and IL-6, both of which can affect barrier function and disease progression (26, 70–73), were greater in septic WT mice relative to septic claudin-2 KO mice. Together, these differences in immune activation could explain reduced local tissue injury, peritoneal bacterial burden, and mortality in claudin-2 KO mice (Table 4).

In addition to the findings in IELs, KO mice had significantly fewer $CD4^+CD69^+$ T cells and decreased numbers of both $CD4^+CD25^+$ T cells and $CD8^+CD25^+$ T cells in Peyer's Patches. CD69 and CD25 both signal through STAT5 to increase T cell activation and proliferation, and thus their reduction is likely indicative of decreased T cell activation (74). T cell activation is generally considered to be beneficial in the host response to sepsis by allowing cells to proliferate and fight off invading pathogens. However, the presence of fewer activated T cells could potentially result in reduced local cytokine responses, which could also play a role in the survival advantage seen in claudin-2 KO mice.

The microbiome has long been hypothesized to play a key role in survival from sepsis. Microbial diversity decreases and new virulence factors are induced after sepsis (75–78), and changes in microbial composition are associated with mortality in patients with both sepsis and COVID-19 (49, 79). Further, studies with genetically identical mice from different vendors demonstrate the microbiome is mechanistically responsible for changes in sepsis mortality (16). Claudin-2 KO and WT mice had modest basal differences in their microbiome despite the fact that they were kept in the same animal facility throughout their lives and claudin-2 KO mice develop normally. This suggests that altering claudin-2 may lead to bi-directional communication with the gut lumen that triggers changes in microbial composition. Further differences in the microbiome were exaggerated following sepsis. The microbial composition of septic KO and WT mice were distinct from unmanipulated mice of the same genotype and also distinct from each other, suggesting an interplay between claudin-2 and sepsis in modulating the microbiome. Notably cecal slurry experiments demonstrated that the changes in the microbiome contributed to the mortality differences between KO and WT mice, as cecal slurry from septic claudin-2 KO mice given to healthy WT recipients resulted in less mortality relative to cecal slurry from septic WT mice given to healthy WT recipients. The observation that heat inactivating cecal slurry led to 100% survival in both groups reduces the likelihood that other, non-microbial materials within the cecal slurry contributed to mortality differences.

Changes in the microbiome and mortality in claudin-2 KO mice were not replicated by CK2 inhibition using silmitasertib. One potential explanation for this result is that silmitasertib-induced claudin-2 channel inactivation was incomplete, consistent with our previous work showing that the effect of claudin-2 KO is significantly greater than chronic silmitasertib treatment (12). Further, silmitasertib was dosed for 3 d in our baseline studies and 4 d in sepsis studies (three prior to CLP, one after CLP) which was a shorter period of time than was used when dosing treatment than the prior immune-mediated colitis studies. Alternatively, oral

Table 2. Primary antibodies used for immunohistochemistry

Antigen	Host	Source	Clone/Catalog	RRID	Concentration
Claudin-2	Rabbit	Turner lab	Rb188-1/2	AB_2916077	1 μg/mL (IF)
Claudin-3	Rabbit	Thermo fisher scientific	34-1700	AB_86804	1 μg/mL (IF)
Claudin-4	Rabbit	Abcam	ab210796	AB_2732879	0.1 μg/mL (IF)
Claudin-5	Rabbit	BiCell	205		1 μg/mL (IF)
Claudin-7	Rabbit	Abcam	ab207300	AB_2783812	0.5 μg/mL (IF)
Claudin-15	Rabbit	BiCell	215		1 μg/mL (IF)
pMLC	Rabbit	Turner lab	6889+6890	AB_2916078	1 μg/mL (IF)
Occludin	Rat	Turner lab	Clone 6B8A3	AB_2819194	1 μg/mL (IF)
Occludin	Rat	Turner lab	Clone 5E5A6	AB_2819196	1 μg/mL (IF)
E-cadherin	Mouse	Abnova	MAB1388	AB_1671631	1 μg/mL (IF)
NaKATPase	Mouse	SantaCruz	sc-48345	AB_626712	0.5 μg/mL (IF)
ZO-1	Rat	Turner lab	Clone 6B6E4	AB_2783858	0.5 μg/mL (IF)
ZO-1	Rat	Turner lab	Clone R40.76	AB_2783859	0.5 μg/mL (IF)
CD3	Rabbit	Abcam	Ab16669	AB_443425	5 μg/mL (IF)
CD4	Rat	eBioscience	13-9766-82	AB_2572833	5 μg/mL (IF)
CD8	Rat	eBioscience	13-0808-82	AB_2572771	5 μg/mL (IF)
CD25	Mouse	Novus biologicals	NB600-564	AB_10002565	5 μg/mL (IF)
CD68	Mouse	SantaCruz	sc-20060	AB_2891106	1 μg/mL (IF)
F4/80	Rabbit	Cell signaling	70076T	AB_2799771	1 μg/mL (IF)
MPO	Rabbit	Abcam	Ab9535	AB_307322	1 μg/mL (IF)
JAMA	Rabbit	Thermo fisher scientific	36-1700	AB_148483	0.5 μg/mL (IF)
Ki67	Rabbit	Novus biologicals	NB600-1252	AB_2142376	5 μg/mL (IF)
CD3	Rat	BioRad	MCA1477A488	AB_321245	5 μg/mL (IF)
CD8	Rat	Biolegend	372902	AB_2650657	10 μg/mL (IF)

Table 3. Secondary antibodies

Antigen	Host	Source	Clone/Catalog	RRID	Concentration
AF488-anti Mouse IgG $F(ab')_2$	Donkey	Jackson ImmunoResearch	715-546-151	AB_2340850	1 μg/mL
AF488-anti Rabbit IgG $F(ab')_2$	Donkey	Jackson ImmunoResearch	711-545-152	AB_2313584	1 μg/mL
AF488-anti Rat IgG $F(ab')_2$	Donkey	Jackson ImmunoResearch	712-546-153	AB_2340686	1 μg/mL
AF594-anti Mouse IgG $F(ab')_2$	Donkey	Jackson ImmunoResearch	715-586-151	AB_2340858	1 μg/mL
AF594-anti Rabbit IgG $F(ab')_2$	Donkey	Jackson ImmunoResearch	711-586-152	AB_2340622	1 μg/mL
AF594-anti Rat IgG $F(ab')_2$	Donkey	Jackson ImmunoResearch	712-586-153	AB_2340691	1 μg/mL
AF647-anti Mouse IgG $F(ab')_2$	Donkey	Jackson ImmunoResearch	715-606-151	AB_2340866	1 μg/mL
AF647-anti Rabbit IgG $F(ab')_2$	Donkey	Jackson ImmunoResearch	711-606-152	AB_2340625	1 μg/mL
AF647-anti Rat IgG $F(ab')_2$	Donkey	Jackson ImmunoResearch	712-606-153	AB_2340696	1 μg/mL

Table 4. Flow cytometry antibodies

Antibody	Source	Clone/ Catalog	RRID	Concentration
anti-CD3-BV421	Biolegend	100228	AB_2562553	2 μg/mL (Flow)
anti-CD3-APC-Cy7	Biolegend	100222	AB_2242784	2 μg/mL (Flow)
anti-CD4-BV421	Biolegend	100443	AB_2562557	2 μg/mL (Flow)
anti-CD8a-BV510	Biolegend	100752	AB_2563057	2 μg/mL (Flow)
anti-CD8a-BV785	Biolegend	100750	AB_2562610	2 μg/mL (Flow)
anti-CD8b-PE-Dazzle	Biolegend	126622	AB_2632630	2 μg/mL (Flow)
anti-CD19-PerCP	Biolegend	115532	AB_2072926	2 μg/mL (Flow)
anti-Gr1-Alexa 700	Biolegend	108422	AB_2137487	5 μg/mL (Flow)
anti-F4/80-Alexa 488	Biolegend	123120	AB_893479	5 μg/mL (Flow)
anti-CD11b-APC	Biolegend	101212	AB_312795	2 μg/mL (Flow)
anti-CD11c-PE/Cyanine7	Biolegend	117318	AB_493568	2 μg/mL (Flow)
anti-NK1.1-PE	Biolegend	108708	AB_313395	2 μg/mL (Flow)
anti-CD25-FITC	Biolegend	102006	AB_312855	5 μg/mL (Flow)
anti-CD69-APC-Cy7	Biolegend	104526	AB_10679041	2 μg/mL (Flow)
anti-CD44-PerCP	Biolegend	103036	AB_10645506	2 μg/mL (Flow)
anti-CD45-Alexa 700	BD	560693	AB_1727491	2 μg/mL (Flow)
anti-CD62L-PE	Biolegend	104408	AB_313095	2 μg/mL (Flow)
anti-MHCII-APC/Cyanine7	Biolegend	107628	AB_2069377	2 μg/mL (Flow)
anti-TCR γδ-PE	eBioscience	12-5711-82	AB_465934	2 μg/mL (Flow)
anti-TNF-PE/Cyanine7	Biolegend	506324	AB_2256076	2 μg/mL (Flow)
anti-IFN-γ-APC	Biolegend	505810	AB_315404	2 μg/mL (Flow)
anti-IL-17A-Alexa488	Invitrogen	53-7177-81	AB_763579	5 μg/mL (Flow)

absorption is diminished both after sepsis and after abdominal surgery, so it is possible that silmitasertib failed to change the microbiome in the immediate post-operative period in septic mice due to poor absorption. Additionally, it is important to note that silmitasertib is a CK2 inhibitor and not a specific claudin-2 inhibitor and is distributed systemically. As such, the ubiquitous expression and substrate promiscuity of CK2 would be expected to lead to silmitasertib effects entirely unrelated to claudin-2 as CK2 modulates processes in multiple organs and cell types where claudin-2 is not expressed. For instance, CK2 is a key regulator of the immune response as well as osteogenesis, adipogenesis, chondrogenesis, and neuron differentiation (80). CK2 further acts as an important regulator of PI3K–Akt, Jak–Stat, NFκB, Wnt, and DNA repair signaling (81). Specifically in the realm of sepsis, infection and critical illness, dissociation of TNF receptor-associated factor 6 and somatic nuclear autoantigenic sperm protein is blunted after LPS treatment in THP-1 cells treated with CK2 inhibitor (82). Additionally, CK2 inhibition attenuates sepsis-induced acute kidney injury and decreases TNF, IFN-γ, and IL-6 in both blood and peritoneum following CLP (83). In other settings, myeloid-specific CK2 KO results in increased myeloid cell recruitment, activation and resistance following *Listeria monocytogenes* infection (84). Finally, CK2 downregulation after intracerebral hemorrhage contributes to brain injury, which is attenuated by CK2 overexpression (85). Thus, CK2 activation and inhibition have pleiotropic effects on host responses that, for the most part, are independent of claudin-2.

It is important to note that, although we have focused on pore pathway permeability, it is possible that the survival advantage of claudin-2 is due to non-channel claudin-2 functions. For instance, claudin-2 has been associated with increased epithelial proliferation and enhanced mucosal healing (32, 86). There were, however, no baseline differences in epithelial proliferation in KO and WT mice. Further, sepsis decreased epithelial proliferation similarly in KO and WT mice, making it difficult to understand how claudin 2 effects on proliferation could increase survival. Finally, a recent study reported immunohistochemical and flow cytometric detection of claudin-2 in lamina propria HLA-DR$^+$ monocytes and macrophages (87). However, no other groups have reported claudin-2 expression in immune cells, and single-cell RNAseq failed to detect claudin-2 in these cell types (88, 89). Further, the polyclonal claudin-2 antibody used in that study was not antigen affinity-purified and the manufacturer reports using A-431 and HeLa cells, neither of which express claudin-2, as positive controls (90, 91). In contrast, we generated our own antigen affinity-purified rabbit anti-claudin-2 polyclonal antibodies and validated their specificity using claudin-2 KO mouse tissue as well as claudin-2 KO human intestinal epithelial cells. Nonetheless, we cannot rule out an extra-intestinal role for claudin-2. Nevertheless, claudin-2 deletion limits in paracellular permeability increases, microbiome changes, and systemic inflammatory responses in septic mice. Any of these could be responsible for the survival benefit seen.

This study has a number of limitations. We did not perform necropsies on mice that died during the week following CLP and, therefore, cannot know whether the number, size or distribution of abscesses differed between WT and KO mice. We also acknowledge that our focus was on comparisons between groups and did not assess intra-group variation in detail (92). The overlap between WT and claudin-2 KO mice in many figures suggests that other insights might be provided by more careful examination of intra-group differences. Because each individual mouse was analyzed at a single time point, we were not able to determine whether, for example, peritoneal macrophage numbers 24 h after CLP correlated with survival. Thus, there may have been other aspects of mortality that were not detected due to our experimental design. In addition, while we examined the impact of transferring cecal slurry from septic WT and claudin-2 KO mice to healthy donors, we did not perform experiments transferring stool to germ-free mice, which likely would have yielded complementary insights. Further, the cecal slurry experiments used donor mice subjected to CLP, and examining the role of claudin-2 KO in other models of sepsis could yield insights as to how generalizable our findings are. We examined ileum in the human studies because it is often resected as part of a right hemicolectomy, ileocecectomy, or total colectomy while jejunal resections are uncommon. This differed from the studies in mice, where, the jejunum was analyzed. This experimental design was based on data demonstrating that a) claudin-2 was upregulated following CLP in the intestine but not the liver or kidney (which have claudin-2 epithelial expression at baseline) and b) the jejunum is the intestinal segment with the greatest permeability increase following CLP (11). It is possible that claudin-2 directly modifies immune activation and that these differences are responsible for the increased survival of claudin-2 KO mice after CLP. In this case, distinct stress-induced mucosal immune responses might secondarily alter the microbiome (93–97). This model is consistent with our previous work showing that immune-mediated colitis is attenuated by claudin-2 KO (12, 56). Alternatively, effects of claudin-2 on stress-induced dysbiosis may modify mucosal immune activation secondarily. This idea is supported by the observation that Na^+H^+ exchanger 3 (NHE3, *Slc9a3*) deficiency induces dysbiosis (98) as well as many studies showing that the microbiome can modulate mucosal immunity (99–104). Next, the distinct effects of CLP on the microbiome and mucosal immune system may simply reflect more severe disease in WT mice as the result of some other claudin-2-dependent process.

Despite these limitations, the data demonstrate that intestinal epithelial claudin-2 expression is upregulated during human and experimental sepsis and that, in mice, this claudin-2 expression

promotes disease progression and death. Conversely, the remarkable protection afforded by claudin-2 KO suggests that inhibition of claudin-2 functions might be beneficial in sepsis.

Materials and Methods

Additional methodological detail is available in *SI Appendix, Supplementary Materials and Methods*.

Human Tissues. De-identified patient tissues were obtained from the archives of Brigham and Women's Hospital under an IRB-approved exempt protocol. All patients had evidence of organ dysfunction with a SOFA score ≥2, consistent with clinical criteria for sepsis from the Sepsis 3 definition (105). Right hemicolectomies for non-inflammatory processes, primarily adenocarcinoma, from age- and sex-matched patients without serositis served as controls.

Mice. Global claudin-2 KO mice were developed by replacing the 3′ half of the single exon containing the open reading frame with a pgk-neo cassette (29) and maintained under specific pathogen-free conditions.

Sepsis Model. Prior to surgery, a single dose of buprenorphine (0.1 mg/kg, McKesson Medical, San Francisco, CA) was given to all mice. Mice were then subjected to CLP or sham laparotomy (106). Since septic patients receive antibiotics and fluid resuscitation (3), mice received ceftriaxone (50 mg/kg, Sigma-Aldrich, St. Louis, MO) and metronidazole (30 mg/kg, Apotex Corp, Weston, FL) subcutaneously after CLP and every 12 h thereafter for four total doses as well as 1 mL of normal saline post-operatively.

Pharmacological CK2 Inhibition. Mice were randomized to receive either silmitasertib via oral gavage or an equivalent volume of PBS. For microbiome studies, separate cohorts of control and septic WT mice received silmitasertib or PBS every 12 h beginning 72 h prior to CLP, at the time of CLP, and 12 h after CLP. Sacrifice was at 24 h post CLP (12). For survival studies, mice received silmitasertib or PBS every 12 h beginning 72 h prior to CLP, at the time of CLP, and every 12 h after CLP for a total of 7 doses (out to 84 h). Mice were followed for survival for 120 h.

Histomorphometry and Immunochemistry. Hematoxylin and eosin stained tissue sections were used to assess villus length and Chiu's mucosal injury score (107). For multiplex immunostaining, formalin-fixed, paraffin-embedded tissues were assembled into tissue microarrays. Tiled images were collected using a semi-automated imaging protocol (108) and quantitative morphometry was performed using Cell Profiler (109).

Flow Cytometry. Spleens and Peyer's patches were harvested and gently smashed into single-cell suspensions. For peritoneal fluid, 1 mL of normal saline with counting beads was injected into the intraperitoneal cavity and a cell pellet was recovered by centrifugation. IELs

Cecal Slurry. WT and claudin-2 KO mice were made septic via CLP and sacrificed 24 h later to serve as cecal slurry donors. After mice were sacrificed, cecal contents from septic mice were extruded into sterile microtubes, weighed, and diluted with sterile saline to a final concentration of 60 mg/mL (110). Cecal slurries were then vortexed to make homogenous solutions. A total of 20 μL/g of either septic WT or claudin-2 KO donor mice-derived cecal slurry solutions was then injected intraperitoneally into healthy WT recipient mice. After the injection, mice were observed every 12 h and followed for survival. To determine whether the mortality difference in the cecal slurry experiment was due to components other than viable bacteria, slurries were heat inactivated in a separate set of experiments. All experimental conditions were identical except heat inactivation was performed by incubating the prepared cecal slurry at 72 °C for 10 min (111).

Statistical Analysis. Data are presented as mean ± SD or absolute numbers and percentages as appropriate.

Study Approval. All experimental procedures on mice were conducted consistent with the NIH Guidelines for the Use of Laboratory Animals and were approved by the Institutional Animal Care and Use Committee at Emory University School of Medicine (Protocol 201800033). An exempt protocol was approved by the IRB at Brigham and Women's Hospital for de-identified human pathologic specimens.

Data, Materials, and Software Availability. All study data are included in the article and/or *SI Appendix*.

ACKNOWLEDGMENTS. This work was supported by the U.S. NIH, grants GM148217 (C.M.C.), GM072808 (C.M.C.), AI149724 (M.L.F.), DK061931 (J.R.T.), DK68271 (J.R.T.), and P30DK034854 (the Harvard Digestive Disease Center), and US Department of Defense award PR181271 (J.R.T.). We thank Jerome Anyalebechi and David Swift for intellectual input into the final manuscript.

Author affiliations: [a]Department of Surgery and Emory Critical Care Center, Emory University School of Medicine, Atlanta, GA 30322; [b]Department of Emergency and Critical Care Medicine, Chiba University Graduate School of Medicine, Chiba 260-8670, Japan; [c]Laboratory of Mucosal Pathobiology, Department of Pathology, Brigham and Women's Hospital and Harvard Medical School, Boston, MA 02115; [d]Department of Pathology and Laboratory Medicine, Emory University School of Medicine, Atlanta, GA 30322; [e]Epithelial Biology Center, Department of Surgery, Vanderbilt University Medical Center, Nashville, TN 37240; [f]Advanced Comprehensive Research Organization, Teikyo University, Tokyo 173-0003, Japan; and [g]Department of Surgery and Emory Transplant Center, Emory University School of Medicine, Atlanta, GA 30322

1. K. E. Rudd *et al.*, Global, regional, and national sepsis incidence and mortality, 1990–2017: Analysis for the Global Burden of Disease Study. *Lancet* **395**, 200–211 (2020).
2. T. G. Buchman *et al.*, Sepsis among medicare beneficiaries: 1. The burdens of sepsis, 2012–2018. *Crit. Care Med.* **48**, 276–288 (2020).
3. L. Evans *et al.*, Surviving sepsis campaign: International guidelines for management of sepsis and septic shock 2021. *Crit. Care Med.* **49**, e1063–e1143 (2021).
4. M. M. Levy *et al.*, Mortality changes associated with mandated public reporting for sepsis. The results of the New York State initiative. *Am. J. Respir. Crit. Care Med.* **198**, 1406–1412 (2018).
5. C. A. Santacruz, A. J. Pereira, E. Celis, J. L. Vincent, Which multicenter randomized controlled trials in critical care medicine have shown reduced mortality? A systematic review. *Crit. Care Med.* **47**, 1680–1691 (2019).
6. S. Otani, C. M. Coopersmith, Gut integrity in critical illness. *J. Intensive Care* **7**, 17 (2019).
7. K. T. Fay, M. L. Ford, C. M. Coopersmith, The intestinal microenvironment in sepsis. *Biochim. Biophys. Acta Mol. Basis Dis.* **1863**, 2574–2583 (2017).
8. R. Mittal, C. M. Coopersmith, Redefining the gut as the motor of critical illness. *Trends Mol. Med.* **20**, 214–223 (2014).
9. R. Sender, S. Fuchs, R. Milo, Are we really vastly outnumbered? Revisiting the ratio of bacterial to host cells in humans. *Cell* **164**, 337–340 (2016).
10. M. A. Odenwald, J. R. Turner, The intestinal epithelial barrier: A therapeutic target? *Nat. Rev. Gastroenterol. Hepatol.* **14**, 9–21 (2017).
11. B. P. Yoseph *et al.*, Mechanisms of intestinal barrier dysfunction in sepsis. *Shock* **46**, 52–59 (2016).
12. P. Raju *et al.*, Inactivation of paracellular cation-selective claudin-2 channels attenuates immune-mediated experimental colitis in mice. *J. Clin. Invest.* **130**, 5197–5208 (2020).
13. L. Zuo, W. T. Kuo, J. R. Turner, Tight junctions as targets and effectors of mucosal immune homeostasis. *Cell. Mol. Gastroenterol. Hepatol.* **10**, 327–340 (2020).
14. J. C. Alverdy, J. N. Luo, The influence of host stress on the mechanism of infection: Lost microbiomes, emergent pathobiomes, and the role of interkingdom signaling. *Front. Microbiol.* **8**, 322 (2017).
15. G. D. Kitsios *et al.*, Dysbiosis in the intensive care unit: Microbiome science coming to the bedside. *J. Crit. Care* **38**, 84–91 (2017).
16. K. T. Fay *et al.*, The gut microbiome alters immunophenotype and survival from sepsis. *FASEB J.* **33**, 11258–11269 (2019).
17. T. Hilbert *et al.*, Vendor effects on murine gut microbiota influence experimental abdominal sepsis. *J. Surg. Res.* **211**, 126–136 (2017).
18. J. Cabrera-Perez *et al.*, Gut microbial membership modulates CD4 T cell reconstitution and function after sepsis. *J. Immunol.* **197**, 1692–1698 (2016).
19. J. R. Turner, Intestinal mucosal barrier function in health and disease. *Nat. Rev. Immunol.* **9**, 799–809 (2009).
20. K. Mineta *et al.*, Predicted expansion of the claudin multigene family. *FEBS Lett.* **585**, 606–612 (2011).
21. M. Furuse, K. Fujita, T. Hiiragi, K. Fujimoto, S. Tsukita, Claudin-1 and -2: Novel integral membrane proteins localizing at tight junctions with no sequence similarity to occludin. *J. Cell Biol.* **141**, 1539–1550 (1998).
22. A. S. Yu *et al.*, Molecular basis for cation selectivity in claudin-2-based paracellular pores: Identification of an electrostatic interaction site. *J. Gen. Physiol.* **133**, 111–127 (2009).
23. P. Y. Tsai *et al.*, IL-22 upregulates epithelial claudin-2 to drive diarrhea and enteric pathogen clearance. *Cell Host Microbe* **21**, 671–681 (2017).
24. F. Heller *et al.*, Interleukin-13 is the key effector Th2 cytokine in ulcerative colitis that affects epithelial tight junctions, apoptosis, and cell restitution. *Gastroenterology* **129**, 550–564 (2005).
25. J. Mankertz *et al.*, TNFalpha up-regulates claudin-2 expression in epithelial HT-29/B6 cells via phosphatidylinositol-3-kinase signaling. *Cell Tissue Res.* **336**, 67–77 (2009).
26. T. Suzuki, N. Yoshinaga, S. Tanabe, Interleukin-6 (IL-6) regulates claudin-2 expression and tight junction permeability in intestinal epithelium. *J. Biol. Chem.* **286**, 31263–31271 (2011).
27. L. Pei *et al.*, Paracellular epithelial sodium transport maximizes energy efficiency in the kidney. *J. Clin. Invest.* **126**, 2509–2518 (2016).
28. M. Wada, A. Tamura, N. Takahashi, S. Tsukita, Loss of claudins 2 and 15 from mice causes defects in paracellular Na+ flow and nutrient transport in gut and leads to death from malnutrition *Gastroenterology* **144**, 369–380 (2013).
29. S. Muto *et al.*, Claudin-2-deficient mice are defective in the leaky and cation-selective paracellular permeability properties of renal proximal tubules. *Proc. Natl. Acad. Sci. U.S.A.* **107**, 8011–8016 (2010).

30. A. Tamura *et al.*, Loss of claudin-15, but not claudin-2, causes Na+ deficiency and glucose malabsorption in mouse small intestine. *Gastroenterology* **140**, 913–923 (2011).
31. R. Ahmad *et al.*, Claudin-2 protects from colitis-associated cancer by promoting colitis-associated mucosal healing. *J. Clin. Invest.* **133**, e170771 (2023), 10.1172/jci170771.
32. R. Ahmad *et al.*, Targeted colonic claudin-2 expression renders resistance to epithelial injury, induces immune suppression, and protects from colitis. *Mucosal Immunol.* **7**, 1340–1353 (2014).
33. Q. Li *et al.*, Disruption of tight junctions during polymicrobial sepsis in vivo. *J. Pathol.* **218**, 210–221 (2009).
34. W. Wang *et al.*, Intestinal alkaline phosphatase inhibits the translocation of bacteria of gut-origin in mice with peritonitis: Mechanism of action. *PLoS One* **10**, e0124835 (2015).
35. L. Khailova, C. H. Baird, A. A. Rush, C. Barnes, P. E. Wischmeyer, Lactobacillus rhamnosus GG treatment improves intestinal permeability and modulates inflammatory response and homeostasis of spleen and colon in experimental model of Pseudomonas aeruginosa pneumonia. *Clin. Nutr.* **36**, 1549–1557 (2017).
36. B. Obermüller *et al.*, Examination of intestinal ultrastructure, bowel wall apoptosis and tight junctions in the early phase of sepsis. *Sci. Rep.* **10**, 11507 (2020).
37. R. Quan *et al.*, BAFF blockade attenuates inflammatory responses and intestinal barrier dysfunction in a murine endotoxemia model. *Front. Immunol.* **11**, 570920 (2020).
38. S. Otani *et al.*, Overexpression of BCL-2 in the intestinal epithelium prevents sepsis-induced gut barrier dysfunction via altering tight junction protein expression. *Shock* **54**, 330–336 (2020).
39. J. Fu, G. Li, X. Wu, B. Zang, Sodium butyrate ameliorates intestinal injury and improves survival in a rat model of cecal ligation and puncture-induced sepsis. *Inflammation* **42**, 1276–1286 (2019).
40. V. L. Jorgensen, S. L. Nielsen, K. Espersen, A. Perner, Increased colorectal permeability in patients with severe sepsis and septic shock. *Intensive Care Med.* **32**, 1790–1796 (2006).
41. C. R. Weber *et al.*, Epithelial myosin light chain kinase activation induces mucosal interleukin-13 expression to alter tight junction ion selectivity. *J. Biol. Chem.* **285**, 12037–12046 (2010).
42. K. Morita, H. Sasaki, M. Furuse, S. Tsukita, Endothelial Claudin. Claudin-5/TMVCF constitutes tight junction strands in endothelial cells. *J. Cell Biol.* **147**, 185–194 (1999).
43. N. Rajagopal, F. J. Irudayanathan, S. Nangia, Palmitoylation of claudin-5 proteins influences their lipid domain affinity and tight junction assembly at the blood-brain barrier interface. *J. Phys. Chem. B* **123**, 983–993 (2019).
44. P. D. Thompson *et al.*, Claudin 13, a member of the claudin family regulated in mouse stress induced erythropoiesis. *PLoS One* **5**, e12667 (2010).
45. S. D. Chanez-Paredes, S. Abtahi, W.-T. Kuo, J. R. Turner, "Differentiating between tight junction-dependent and tight junction-independent intestinal barrier loss in vivo" in *Methods in Molecular Biology*, K. Turksen, Ed. (Humana, New York, NY, 2021), vol. 2367.
46. D. R. Clayburgh *et al.*, Epithelial myosin light chain kinase-dependent barrier dysfunction mediates T cell activation-induced diarrhea in vivo. *J. Clin. Invest.* **115**, 2702–2715 (2005).
47. L. Su *et al.*, TNFR2 activates MLCK-dependent tight junction dysregulation to cause apoptosis-mediated barrier loss and experimental colitis. *Gastroenterology* **145**, 407–415 (2013).
48. W. V. Graham *et al.*, Intracellular MLCK1 diversion reverses barrier loss to restore mucosal homeostasis. *Nat. Med.* **25**, 690–700 (2019).
49. R. Prevel *et al.*, Gut bacteriobiota and mycobiota are both associated with Day-28 mortality among critically ill patients. *Crit. Care* **26**, 105 (2022).
50. J. Schlechte *et al.*, Dysbiosis of a microbiota-immune metasystem in critical illness is associated with nosocomial infections. *Nat. Med.* **29**, 1017–1027 (2023), 10.1038/s41591-023-02243-5.
51. J. C. Alverdy, M. A. Krezalek, Collapse of the microbiome, emergence of the pathobiome, and the immunopathology of sepsis. *Crit. Care Med.* **45**, 337–347 (2017).
52. X. Long *et al.*, Global signatures of the microbiome and metabolome during hospitalization of septic patients. *Shock* **59**, 716–724 (2023), 10.1097/shk.0000000000002117.
53. M. J. Carvalho *et al.*, Antibiotic resistance genes in the gut microbiota of mothers and linked neonates with or without sepsis from low- and middle-income countries. *Nat. Microbiol.* **7**, 1337–1347 (2022).
54. X. Chen *et al.*, Pregnancy-induced changes to the gut microbiota drive macrophage pyroptosis and exacerbate septic inflammation. *Immunity* **56**, 336–352.e9 (2023).
55. J. F. Colbert *et al.*, Aging-associated augmentation of gut microbiome virulence capability drives sepsis severity. *mBio* **14**, e00052-23 (2023).
56. D. R. Raleigh *et al.*, Occludin S408 phosphorylation regulates tight junction protein interactions and barrier function. *J. Cell Biol.* **193**, 565–582 (2011).
57. L. Kong, P. Wu, J. Li, miR-331 inhibits CLDN2 expression and may alleviate the vascular endothelial injury induced by sepsis. *Exp. Ther. Med.* **20**, 1343–1352 (2020).
58. M. Ong, S. Yeruva, A. Sailer, S. P. Nilsen, J. R. Turner, Differential regulation of claudin-2 and claudin-15 expression in children and adults with malabsorptive disease. *Lab. Invest.* **100**, 483–490 (2020).
59. S. Sipola *et al.*, Colon epithelial injury in critically ill colectomized patients: Aberration of tight junction proteins and Toll-like receptors. *Minerva Anestesiol.* **83**, 1017–1025 (2017).
60. J. A. Clark *et al.*, Enterocyte-specific epidermal growth factor prevents barrier dysfunction and improves mortality in murine peritonitis. *Am. J. Physiol. Gastrointest. Liver Physiol.* **297**, G471–G479 (2009).
61. L. Bird, T cells: IL-9 breaks down barriers. *Nat. Rev. Immunol.* **14**, 432 (2014).
62. C. M. Van Itallie *et al.*, The density of small tight junction pores varies among cell types and is increased by expression of claudin-2. *J. Cell Sci.* **121**, 298–305 (2008).
63. W. T. Kuo *et al.*, Inflammation-induced occludin downregulation limits epithelial apoptosis by suppressing caspase-3 expression. *Gastroenterology* **157**, 1323–1337 (2019).
64. R. S. Hotchkiss *et al.*, Rapid onset of intestinal epithelial and lymphocyte apoptotic cell death in patients with trauma and shock. *Crit. Care Med.* **28**, 3207–3217 (2000).
65. C. M. Coopersmith *et al.*, Inhibition of intestinal epithelial apoptosis and survival in a murine model of pneumonia-induced sepsis. *JAMA* **287**, 1716–1721 (2002).
66. C. M. Coopersmith *et al.*, Overexpression of Bcl-2 in the intestinal epithelium improves survival in septic mice. *Crit. Care Med.* **30**, 195–201 (2002).
67. D. Merlin *et al.*, hPepT1-mediated epithelial transport of bacteria-derived chemotactic peptides enhances neutrophil-epithelial interactions. *J. Clin. Invest.* **102**, 2011–2018 (1998).
68. Y. Liu, X. Wang, L. Yu, Th17, rather than Th1 cell proportion, is closely correlated with elevated disease severity, higher inflammation level, and worse prognosis in sepsis patients. *J. Clin. Lab. Anal.* **35**, e23753 (2021).
69. Q. Zou, C. Liu, N. Hu, W. Wang, H. Wang, miR-126 ameliorates multiple organ dysfunction in septic rats by regulating the differentiation of Th17/Treg. *Mol. Biol. Rep.* **49**, 2985–2998 (2022).
70. R. Al-Sadi, D. Ye, H. M. Said, T. Y. Ma, IL-1beta-induced increase in intestinal epithelial tight junction permeability is mediated by MEKK-1 activation of canonical NF-kappaB pathway. *Am. J. Pathol.* **177**, 2310–2322 (2010).
71. T. Secher *et al.*, Crucial role of TNF receptors 1 and 2 in the control of polymicrobial sepsis. *J. Immunol.* **182**, 7855–7864 (2009).
72. S. Lv *et al.*, Anti-TNF-alpha therapy for patients with sepsis: A systematic meta-analysis. *Int. J. Clin. Pract.* **68**, 520–528 (2014).
73. A. Zahs *et al.*, Inhibition of long myosin light-chain kinase activation alleviates intestinal damage after binge ethanol exposure and burn injury. *Am. J. Physiol. Gastrointest. Liver Physiol.* **303**, G705–712 (2012).
74. P. Martin *et al.*, CD69 association with Jak3/Stat5 proteins regulates Th17 cell differentiation. *Mol. Cell Biol.* **30**, 4877–4889 (2010).
75. M. A. Krezalek, J. Defazio, O. Zaborina, A. Zaborin, J. C. Alverdy, The shift of an intestinal "microbiome" to a "pathobiome" governs the course and outcome of sepsis following surgical injury. *Shock* **45**, 475–482 (2016).
76. D. McDonald *et al.*, Extreme dysbiosis of the microbiome in critical illness. *mSphere* **1**, e00199-16 (2016).
77. N. J. Klingensmith, C. M. Coopersmith, Gut microbiome in sepsis. *Surg. Infect. (Larchmt)* **24**, 250–257 (2023).
78. J. Schlechte *et al.*, Dysbiosis of a microbiota-immune metasystem in critical illness is associated with nosocomial infections. *Nat. Med.* **29**, 1017–1027 (2023).
79. M. Trøseid *et al.*, Gut microbiota composition during hospitalization is associated with 60-day mortality after severe COVID-19. *Crit. Care* **27**, 69 (2023).
80. D. Halloran, V. Pandit, A. Nohe, The role of protein kinase CK2 in development and disease progression: A critical review. *J. Dev. Biol.* **10**, 31 (2022).
81. Ø. Bruserud, H. Reikvam, Casein kinase 2 (CK2): A possible therapeutic target in acute myeloid leukemia. *Cancers (Basel)* **15**, 3711 (2023).
82. F. M. Yang *et al.*, sNASP inhibits TLR signaling to regulate immune response in sepsis. *J. Clin. Invest.* **128**, 2459–2472 (2018).
83. J. H. Koo, H. C. Yu, S. Nam, D. C. Kim, J. H. Lee, Casein kinase 2 alpha inhibition protects against sepsis-induced acute kidney injury. *Int. J. Mol. Sci.* **24**, 9783 (2023).
84. S. R. Larson *et al.*, Myeloid cell CK2 regulates inflammation and resistance to bacterial infection. *Front. Immunol.* **11**, 590266 (2020).
85. Z. Sun *et al.*, Casein kinase 2 attenuates brain injury induced by intracerebral hemorrhage via regulation of NR2B phosphorylation. *Front. Cell Neurosci.* **16**, 911973 (2022).
86. F. B. Ahmad, J. A. Cisewski, J. Xu, R. N. Anderson, Provisional mortality data–United States, 2022. *MMWR Morb. Mortal. Wkly. Rep.* **72**, 488–492 (2023).
87. S. Čužić *et al.*, Claudins: Beyond tight junctions in human IBD and murine models. *Front. Pharmacol.* **12**, 682614 (2021).
88. M. Karlsson *et al.*, A single-cell type transcriptomics map of human tissues. *Sci. Adv.* **7**, eabh2169 (2021).
89. M. Uhlen *et al.*, A genome-wide transcriptomic analysis of protein-coding genes in human blood cells. *Science* **366**, eaax9198 (2019).
90. A. Digre, C. Lindskog, The human protein atlas-Integrated omics for single cell mapping of the human proteome. *Protein Sci.* **32**, e4562 (2023).
91. M. Gry *et al.*, Correlations between RNA and protein expression profiles in 23 human cell lines. *BMC Genomics* **10**, 365 (2009).
92. J. C. Alverdy, Letter to the editor: Between-group comparison fallacy. *Surg. Infect. (Larchmt)* **23**, 609 (2022).
93. W. S. Garrett *et al.*, Communicable ulcerative colitis induced by T-bet deficiency in the innate immune system. *Cell* **131**, 33–45 (2007).
94. M. Vijay-Kumar *et al.*, Metabolic syndrome and altered gut microbiota in mice lacking toll-like receptor 5. *Science* **328**, 228–231 (2010), 10.1126/science.1179721.
95. E. Elinav *et al.*, NLRP6 inflammasome regulates colonic microbial ecology and risk for colitis. *Cell* **145**, 745–757 (2011).
96. A. Couturier-Maillard *et al.*, NOD2-mediated dysbiosis predisposes mice to transmissible colitis and colorectal cancer. *J. Clin. Invest.* **123**, 700–711 (2013).
97. X. Yao *et al.*, Remodelling of the gut microbiota by hyperactive NLRP3 induces regulatory T cells to maintain homeostasis. *Nat. Commun.* **8**, 1896 (2017).
98. C. A. Harrison *et al.*, Microbial dysbiosis associated with impaired intestinal Na(+)/H(+) exchange accelerates and exacerbates colitis in ex-germ free mice. *Mucosal Immunol.* **11**, 1329–1341 (2018).
99. K. Z. Sanidad *et al.*, Maternal gut microbiome-induced IgG regulates neonatal gut microbiome and immunity. *Sci. Immunol.* **7**, eabh3816 (2022).
100. X. Song *et al.*, Microbial bile acid metabolites modulate gut RORgamma(+) regulatory T cell homeostasis. *Nature* **577**, 410–415 (2020).
101. Y. Mishima *et al.*, Microbiota maintain colonic homeostasis by activating TLR2/MyD88/PI3K signaling in IL-10-producing regulatory B cells. *J. Clin. Invest.* **129**, 3702–3716 (2019).
102. K. L. Edelblum *et al.*, The microbiome activates CD4 T-cell–mediated immunity to compensate for increased intestinal permeability. *Cell. Mol. Gastroenterol. Hepatol.* **4**, 285–297 (2017).
103. K. Brandl, G. Plitas, B. Schnabl, R. P. DeMatteo, E. G. Pamer, MyD88-mediated signals induce the bactericidal lectin RegIII gamma and protect mice against intestinal Listeria monocytogenes infection. *J. Exp. Med.* **204**, 1891–1900 (2007).
104. H. L. Cash, C. V. Whitham, C. L. Behrendt, L. V. Hooper, Symbiotic bacteria direct expression of an intestinal bactericidal lectin. *Science* **313**, 1126–1130 (2006).
105. M. Singer *et al.*, The third international consensus definitions for sepsis and septic shock (sepsis-3). *JAMA* **315**, 801–810 (2016).
106. C. C. Baker, I. H. Chaudry, H. O. Gaines, A. E. Baue, Evaluation of factors affecting mortality rate after sepsis in a murine cecal ligation and puncture model. *Surgery* **94**, 331–335 (1983).
107. C. J. Chiu, A. H. McArdle, R. Brown, H. J. Scott, F. N. Gurd, Intestinal mucosal lesion in low-flow states. I. A morphological, hemodynamic, and metabolic reappraisal. *Arch. Surg.* **101**, 478–483 (1970).
108. S. Abtahi *et al.*, A simple method for creating a high-content microscope for imaging multiplexed tissue microarrays. *Curr. Protoc.* **1**, e68 (2021).
109. C. McQuin *et al.*, Cell profiler 3.0: Next-generation image processing for biology. *PLoS Biol.* **16**, e2005970 (2018).
110. J. C. Rincon, P. A. Efron, L. L. Moldawer, S. D. Larson, Cecal slurry injection in neonatal and adult mice. *Methods Mol. Biol.* **2321**, 27–41 (2021).
111. M. E. Starr *et al.*, A new cecal slurry preparation protocol with improved long-term reproducibility for animal models of sepsis. *PLoS One* **9**, e115705 (2014).